mater.scichina.com link.springer.com

Published online 28 November 2022 | https://doi.org/10.1007/s40843-022-2240-y
Sci China Mater 2023, 66(3): 955–963

Gluing $Ba_{0.5}Sr_{0.5}Co_{0.8}Fe_{0.2}O_{3-\delta}$ with Co_3O_4 as a cathode for proton-conducting solid oxide fuel cells

Xuan Yang†, Yanru Yin†, Shoufu Yu and Lei Bi*

ABSTRACT **The $Ba_{0.5}Sr_{0.5}Co_{0.8}Fe_{0.2}O_{3-\delta}$ (BSCF) + Co_3O_4 composite material is evaluated as a cathode for proton-conducting solid oxide fuel cells (H-SOFCs), which provides a new strategy to solve the thermal mismatch problem between the cathode and electrolyte without impairing the cathode performance. BSCF is a well-known cathode material for intermediate-temperature SOFCs, but its performance for H-SOFCs is unsatisfactory. One reason for the relatively low performance is the poor contact between the BSCF cathode and the electrolyte due to the high thermal expansion of BSCF. The relatively low melting point of Co_3O_4 is taken in this study as an advantage to bond the BSCF cathode to the electrolyte, mitigating the poor contact problem for the BSCF with the electrolyte. Furthermore, the addition of Co_3O_4 promotes the catalytic activity of the BSCF cathode as demonstrated by experimental studies and first-principles calculations, leading to an impressively high performance of BSCF-based cathodes for H-SOFCs.**

Keywords: $Ba_{0.5}Sr_{0.5}Co_{0.8}Fe_{0.2}O_{3-\delta}$, cathode, proton-conducting oxides, solid oxide fuel cell

INTRODUCTION

Fuel cell technology, which can directly convert chemical energies into electricity, has received considerable attention in the past decades [1,2]. Solid oxide fuel cells (SOFCs) are an important research direction in the fuel cell community, thus becoming one of the most investigated fuel cell types due to their all-solid-state structure and high efficiency [3–5]. Proton-conducting SOFCs (H-SOFCs) have currently become a popular research topic for SOFCs because they can decrease the working temperatures of traditional SOFCs and thus extend the lifetime of fuel cells [6–9]. In addition, fuel dilution is absent for H-SOFCs because water is produced at the cathode side, improving the efficiency of the cell [10]. Most studies conducted in the past two decades have focused on electrolyte materials [11,12] and cathode materials [13–16] for H-SOFCs. Compared with the search for proton-conducting electrolyte materials with a good compromise between conductivity and chemical stability [17,18], an increasing amount of research has currently shifted to the exploration of proper cathode materials for H-SOFCs because cathodes substantially influence the polarization resistance of the cells and thus govern the output of the fuel cells [19–24].

The cathode reaction mechanism for H-SOFCs indicates that the migrations of protons, oxygen ions, and electrons are important to the cathode performance [25,26]. Therefore, the development of triple-conducting cathodes has recently gained remarkable attention [27–30]; thus, some high-performing triple-conducting cathodes have been proposed for H-SOFCs [31,32]. However, the development of triple-conducting cathodes remains in its early stage compared with the traditional SOFC cathodes. In addition, measuring exact proton and oxygen ion conductions in these oxides is still technically challenging [33,34]. Examining the development history of H-SOFC cathodes, some traditional cathodes have been demonstrated to show the desirable performance of H-SOFCs despite the absence of reports on proton conduction for these cathodes [35–37]. This finding implies that the cathode may also demonstrate good performance for H-SOFCs under high oxygen reduction reaction (ORR) activity.

$Ba_{0.5}Sr_{0.5}Co_{0.8}Fe_{0.2}O_{3-\delta}$ (BSCF), a classical cathode for intermediate-temperature SOFCs, has been demonstrated to deliver excellent performance for oxygen ion conducting SOFCs [38]. However, the utilization of BSCF in H-SOFCs is uncommon despite some attempts [39,40] because the performance of BSCF in H-SOFCs is far inferior to that in oxygen-ion-conducting SOFCs (O-SOFCs). The relatively poor performance of BSCF in H-SOFCs is mainly due to the following two factors: the small proton conduction in BSCF under the dry air condition and the high thermal expansion of BSCF, leading to poor contact between the cathode and electrolyte [41]. The use of a composite cathode by mixing BSCF with a proton-conducting oxide could be a solution to the thermal mismatch problem. However, the interdiffusion of Ba element between BSCF and the proton-conducting oxide could be detrimental to the performance of fuel cells [40]. Considering the high catalytic activity of BSCF, predicting that the BSCF could provide decent performance for H-SOFCs if a good contact between BSCF and electrolyte can be achieved is reasonable, and the performance may be further enhanced if the ORR activity of the BSCF-based cathode is further improved.

Co_3O_4 has been used as a catalyst to promote the ORR activity of the cathode for O-SOFCs; it has also been successfully utilized in other catalysts to facilitate their activity [42,43]. Notably, the melting point of Co_3O_4 is relatively low (895°C), and this temperature is close to the co-firing temperature of cathodes during their layer fabrication process. Therefore, it is feasible to melt Co_3O_4 during the co-firing procedure of cathodes and make it a

School of Resource Environment and Safety Engineering, University of South China, Hengyang 421001, China
† These authors contributed equally to this work.
* Corresponding author (emails: lei.bi@usc.edu.cn or bilei81@gmail.com)

glue to adhere the cathode material with the electrolyte. Meanwhile, Co_3O_4 may further improve the catalytic activity of the cathode [44], thus enhancing the performance of the fuel cells. Based on the above considerations, BSCF is coupled with Co_3O_4 to use the melted Co_3O_4 to bond BSCF with the electrolyte and also further promote the catalytic activity of BSCF for H-SOFCs.

EXPERIMENTAL SECTION

BSCF and Co_3O_4 powders were synthesized by a wet chemical route [45]. Citric acid was used as the complexing agent. The preparation details can be found in the previous studies [22,40]. The BSCF and Co_3O_4 powders were respectively calcined at 900 and 600°C for 3 h each to achieve the pure phase. The BSCF + Co_3O_4 mixture was obtained by mixing BSCF and Co_3O_4 at a weight ratio of 8:2. The phase purities of BSCF, Co_3O_4, and BSCF + Co_3O_4 mixture before and after co-firing were examined by X-ray diffraction (XRD). The morphologies and elemental distributions of these powders were observed by using scanning electron microscopy (SEM) coupled with energy-dispersive X-ray spectroscopy. The BSCF + Co_3O_4 mixture was then evaluated as the cathode in comparison with BSCF without Co_3O_4, and the morphologies of the cathode-electrolyte interfaces after co-firing were observed with SEM.

Anode-supported $BaZr_{0.1}Ce_{0.7}Y_{0.2}O_{3-\delta}$ (BCZY) half-cells were fabricated by the conventional co-pressing and co-sintering method, and the co-sintering temperature was set at 1350°C. The NiO + BCZY composite in a weight ratio of 6:4 was used as the anode. The BSCF + Co_3O_4 mixture used as a cathode was deposited on the surface of the sintered BCZY electrolyte, followed by a co-firing procedure at 900°C in the microwave sintering furnace. The cell structure is NiO + BCZY(anode)/BCZY (electrolyte)/BSCF + Co_3O_4(cathode). The cell was then tested with H_2 and static air as the fuel and the oxidant, respectively. The electrochemical performance of the cell was recorded using an electrochemical workstation (Squidstat Plus, Admiral Instruments). The long-term stability test of the cell was conducted by holding the cell at 600°C with an applied current density of 0.4 A cm^{-2}. The cell voltage was then recorded as a function of time.

First-principles calculations were conducted *via* the density functional theory (DFT) method using VASP (Vienna *ab initio* simulation package) [46]. The details for the parameter settings can be found in the previous report [47]. Briefly, the cutoff energy was set to 520 eV, and a gamma-centered 4 × 4 × 4 *k*-point mesh was used. The convergence criteria for energy and force were 10^{-5} eV and 0.05 eV $Å^{-1}$, respectively. For Hubbard's correction, the U_{eff} values of 3.32 and 4 eV were added to Co and Fe, respectively [48]. The surface model was used for the interface constructions and calculations. The (001) surface of BSCF and the (110) surface of Co_3O_4 were cleaved, and the supercell of the surfaces was expanded to make a matching lattice constant between BSCF and Co_3O_4 for the combination. The final supercell for the interface calculations contained 144 atoms. The bottom four layers of each slab were fixed, and the top two layers were relaxed. The formation energy of oxygen vacancy (E_{vo}) was calculated in accordance with $E_{vo} = E_{defect} + \frac{1}{2}E_{O_2} - E_{perfect}$, in which $E_{perfect}$ is the energy of a perfect bulk and E_{defect} is the energy of a bulk with one oxygen atom deficiency. When calculating the E_{vo} at the BSCF/Co_3O_4, one oxygen atom was removed at the interface and then the E_{defect} was calculated accordingly.

RESULTS AND DISCUSSION

The phase purity of the synthesized BSCF and Co_3O_4 was examined by XRD, suggesting the successful preparation of BSCF and Co_3O_4 materials (Figs S1 and S2, respectively). The BSCF + Co_3O_4 mixture must be co-fired during the cathode fabrication; thus, checking the possible reaction between BSCF and Co_3O_4 at high temperatures is necessary. Fig. 1a shows the XRD patterns of the BSCF + Co_3O_4 mixture before and after the cathode co-firing. The co-firing temperature was set at 900°C. Two separated phases, which include BSCF and Co_3O_4, can be detected for the BSCF + Co_3O_4 mixture before and after firing. However, extra peaks corresponding to CoO appear in the XRD pattern of the BSCF + Co_3O_4 after firing. The appearance of CoO is due to the release of O_2 for Co_3O_4 at high temperatures. By comparing the peaks of BSCF and Co_3O_4 before and after firing, no evident peak shift can be found, suggesting the absence of a reaction between BSCF and Co_3O_4. However, some decomposition of Co_3O_4 to CoO is observed at high temperatures. The Co_3O_4 is still the majority of the cobalt oxides that can be observed from the relative intensity of the Co_3O_4 and CoO peaks. Figs S3 and S4 show the morphologies and the elemental distribution of BSCF and Co_3O_4, respectively. Only Ba, Sr, Co, Fe, and O elements are observed for BSCF, and the distribution of each element is homogeneous without evident accumulation of any element. The same phenomenon is observed for Co_3O_4, wherein no segregation of any element can be found. By contrast, the SEM mapping results for the BSCF + Co_3O_4 mixture after firing shown in Fig. 1b exhibit some difference. Evident accumulation of Co elements at some places can also be observed. BSCF contains Co element, but the Co accumulation phenomenon indicates the abundance of Co at these places, suggesting the existence of cobalt oxides. This result is consistent with the XRD analysis.

One major motivation for coupling Co_3O_4 with BSCF is to use the relatively low melting point of Co_3O_4 that can bond BSCF with the electrolyte layer as a "glue". Fig. 2a shows the co-firing scheme of the BSCF cathode with the electrolyte for the fuel cell fabrications. The BSCF cathode slurry is deposited on the surface of the $BaCe_{0.7}Zr_{0.1}Y_{0.2}O_{3-\delta}$ (BCZY) electrolyte membrane, followed by a co-firing procedure. However, BSCF delaminates from the electrolyte layer due to the well-known high thermal expansion coefficient (TEC) of BSCF [49]. The corresponding SEM image for the BSCF-BCZY interface confirms the poor contact between the single-phase BSCF cathode and the BCZY electrolyte. The BSCF layer completely peels off from the electrolyte layer after co-firing, and a gap is found between the BSCF cathode and BCZY electrolyte parts even after co-firing. By contrast, contact is substantially improved when the BSCF + Co_3O_4 composite cathode is used. Notably, the TEC of Co_3O_4 is even higher than that for BSCF at high temperatures [50]. Therefore, the improved contact for the BSCF + Co_3O_4 composite cathode with the electrolyte cannot come from the balanced TEC by the addition of Co_3O_4. As plotted in Fig. 2b, the dispersed Co_3O_4 melts during the cathode-electrolyte co-firing procedure and then glues the BSCF layer to the electrolyte, avoiding the delamination of the BSCF layer from the electrolyte. The SEM image of the BSCF + Co_3O_4-BCZY interface indicates that the BSCF + Co_3O_4 composite cathode adheres firmly with the electrolyte, thereby solving the delamination

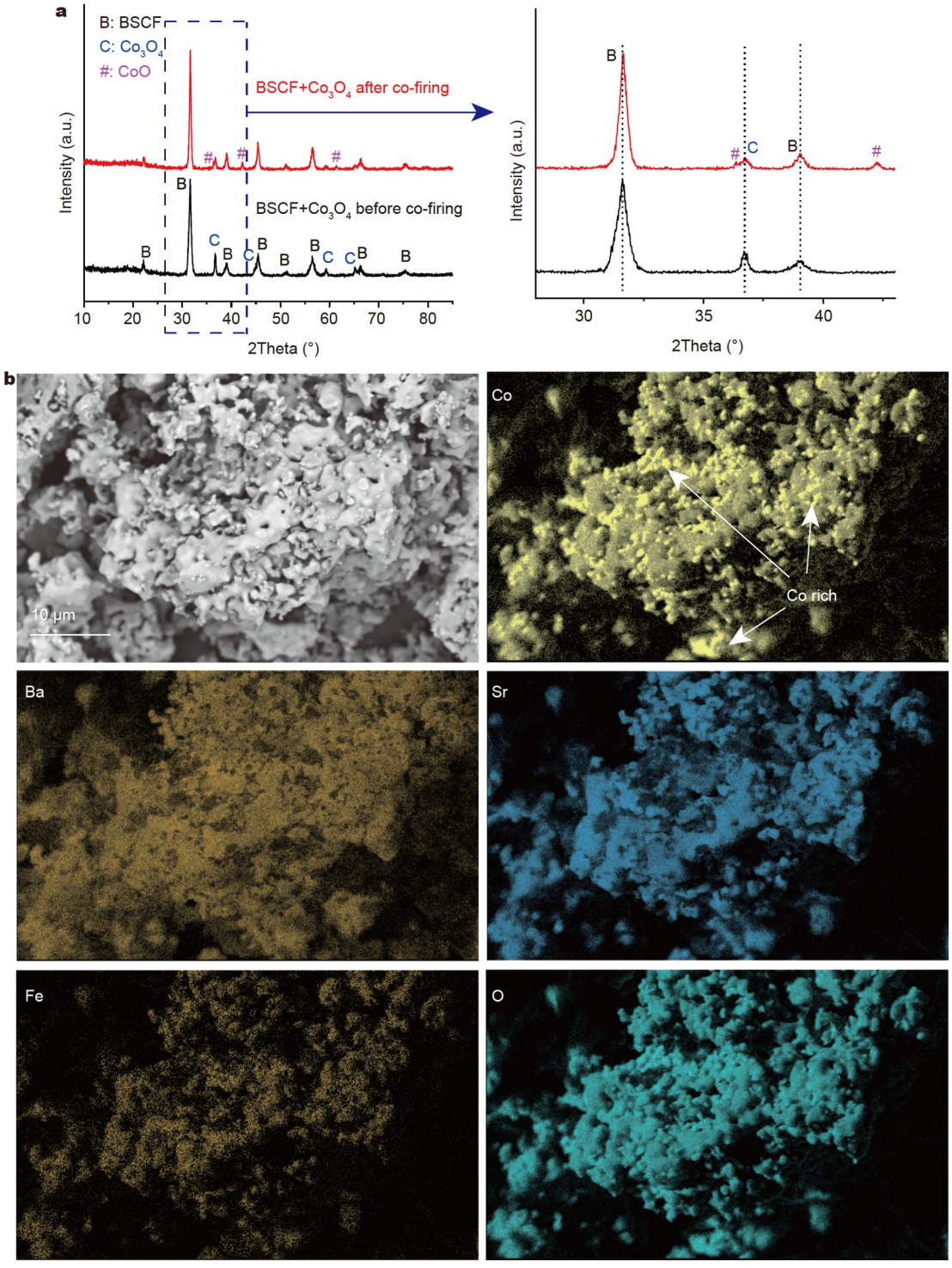

Figure 1 (a) XRD patterns for BSCF + Co_3O_4 mixture before and after firing; (b) SEM image for BSCF + Co_3O_4 mixture powders and their corresponding elemental mapping results.

problem of the BSCF cathode layer. By observing the elemental distribution, although no accumulation of Ba, Sr, and Fe elements can be found for the BSCF + Co_3O_4 cathode, noticeable accumulations of Co elements can be observed in the entire cathode. This phenomenon indicates that Co_3O_4 particles are dispersed in the entire cathode area, which is vital for improving the overall cathode catalytic activity, which will be discussed later. In addition, some Co accumulation can be detected at the cathode-electrolyte interface, which probably plays a critical role in bonding the BSCF layer to the electrolyte layer once Co_3O_4 starts to melt. The relatively low melting point of Co_3O_4 allows this material to melt during the high-temperature firing process, serving as a glue to adhere the BSCF to the BCZY electrolyte layer and overcoming the delamination problem induced by the high TEC of BSCF. If the co-firing temperature is lower than the melting point of Co_3O_4 (such as 800°C), then the BSCF + Co_3O_4

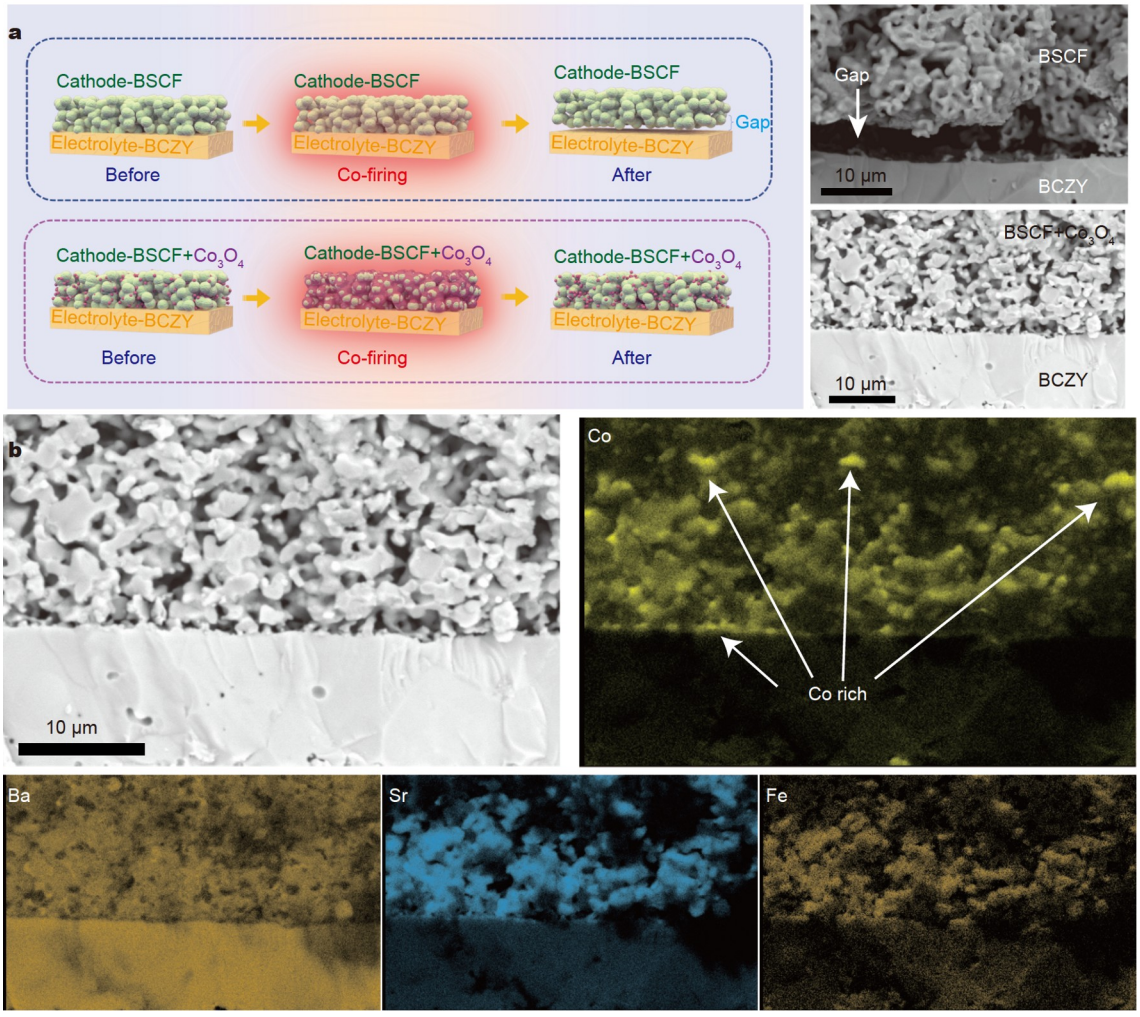

Figure 2 (a) Schematic illustration of the co-firing procedure for BSCF and BSCF + Co_3O_4 cathodes with the electrolyte layer. Their corresponding SEM images for the cross-sectional view are presented. (b) The SEM image for the BSCF + Co_3O_4 cathode and BCZY electrolyte interface with their corresponding elemental mapping analysis.

cathode cannot bond well with the BCZY electrolyte, as shown in Fig. S5. This result further confirms that the melted Co_3O_4 is necessary for bonding the cathode layer to the electrolyte.

The addition of Co_3O_4 solves the thermal mismatch problem between BSCF and the electrolyte. Moreover, Co_3O_4 is found to further promote the catalytic activity of BSCF. Experimental studies were performed to investigate the oxygen diffusion and surface exchange capabilities of BSCF with and without Co_3O_4. The electrical conductivity relaxation (ECR) tests were conducted by abruptly changing the atmosphere from air to 50% O_2, and the conductivity of the material changes until reaching an equilibrium. The relaxation time was recorded, and the results are shown in Fig. 3a, b. The relaxation time is reduced for BSCF with the addition of Co_3O_4. By fitting the ECR data, the oxygen diffusion coefficient (D^*) and the oxygen surface exchange coefficient (k^*) for BSCF + Co_3O_4 are 8.38×10^{-5} cm^2 s^{-1} and 1.02×10^{-3} cm s^{-1}, respectively. These values are significantly increased compared with BSCF (6.98×10^{-5} cm^2 s^{-1} for D^* and 5.52×10^{-4} cm s^{-1} for k^*). The enhanced D^* and k^* values are expected because reports have indicated that the addition of Co_3O_4 can promote the ORR activity of SOFC cathodes [44,51]. The XPS analysis shown in Fig. 3c, d indicates that the BSCF + Co_3O_4 composite cathode has more oxygen vacancies (Vo) than the BSCF. Reports have also indicated that the ratio between the adsorbed and lattice oxygen reflects the Vo content [52,53], and this ratio is 4.9 and 6 for BSCF and BSCF + Co_3O_4, respectively, suggesting that the addition of Co_3O_4 improves the Vo content.

First-principles calculations were used to further explore the formation of Vo at the atomic level. Fig. 4a shows the calculated configuration of the BSCF-Co_3O_4 structure. Reports have indicated that the heterostructure could enhance the interface properties [54]. Therefore, the Vo formation energy (E_{vo}) at the BSCF-Co_3O_4 interface was calculated, and the result indicates that the E_{vo} at the BSCF-Co_3O_4 interface is −2.98 eV, which is significantly lower than that for BSCF (−1.19 eV), suggesting that the formation of Vo is more favorable at the BSCF-Co_3O_4 interface compared with BSCF. This result is consistent with the XPS analysis. Notably, different sites for the Vo formation were calculated, and the formation energy at the BSCF site at the interface has lower energy than that at the Co_3O_4 site, which means the formation of Vo is more favorable at the BSCF site. Reports indicated that the high deficiency of Vo is one of the key reasons for the high ORR activity of BSCF [38]. The improved Vo formation at the BSCF-Co_3O_4 interface further implies ORR

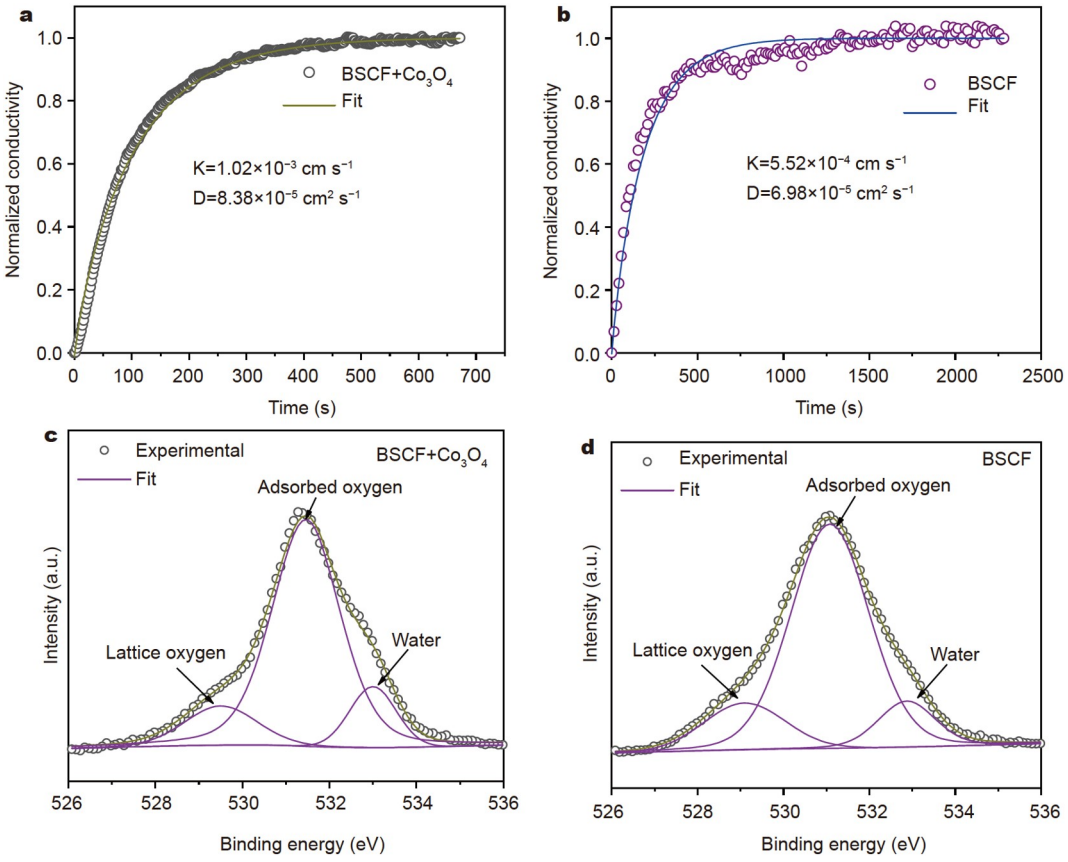

Figure 3 ECR results for (a) BSCF + Co_3O_4 and (b) BSCF cathodes on the change of atmosphere from air to 50% O_2 tested at 600°C; XPS O 1s spectra for (c) BSCF + Co_3O_4 and (d) BSCF.

activity because Vo influences the oxygen ion diffusion and remarkably impacts ORR [55,56]. In addition, the investigation on density of states (DOS) of O 2p and Co 3d, respectively shown in Fig. 4b, c, indicates that the distance between O 2p and Co 3d ($D_{3d\text{-}2p}$) decreases from 3.34 for BSCF to 1.59 for BSCF + Co_3O_4. Report has also indicated that the decreased $D_{3d\text{-}2p}$ distance predicts the low energy formation of Vo [54], which agrees with the aforementioned E_{vo} results. Furthermore, although $D_{3d\text{-}2p}$ is usually regarded as a good indicator of the catalyst activity at room temperature [57] and is not widely used for SOFCs, a recent study indicates that one mechanism for H-SOFC cathode reactions also contains the formation of $*O_2$, *OOH, *O and *OH adsorbates [58], which shows some similarities to the ORR procedure at room temperature [57]. Therefore, the $D_{3d\text{-}2p}$ distance is expected to be useful in predicting the ORR activity for the cathodes of H-SOFCs at intermediate temperatures [54]. The reduced $D_{3d\text{-}2p}$ could facilitate the charge transfer and gas adsorption and desorption [59], thus positively contributing to the ORR activity.

The above experimental and theoretical studies indicate that Co_3O_4 can act as a glue to bond the BSCF cathode to the electrolyte layer due to its low melting point, overcoming the thermal mismatch problem of BSCF. Moreover, the addition of Co_3O_4 could further enhance the ORR activity of BSCF, making it a potential high-performing cathode composition for H-SOFCs. Therefore, the BSCF + Co_3O_4 mixture was evaluated as the cathode for H-SOFCs with the BCZY proton-conducting electrolyte. Fig. 5a shows the current density-voltage (*I-V*) and power density curves for an H-SOFC using a BSCF + Co_3O_4 cathode. The peak power density (PPD) of the cell is 1446, 1089, and 751 mW cm^{-2} at 700, 650, and 600°C, respectively. The fuel cell performance is high even when compared with the recently developed cathodes for H-SOFCs. Further comparing the cell performance with an H-SOFC using the traditional BSCF + BCZY composite cathode, the PPD of the cell using the traditional BSCF + BCZY composite cathode is 1001, 605, and 393 mW cm^{-2} at 700, 650, and 600°C, respectively (Fig. S6). The PPD is lower than that for the cell using the composite BSCF + Co_3O_4 cathode, showing the advantage of the composite BSCF + Co_3O_4 cathode over the conventional BSCF + BCZY composite cathode. In addition, the weight ratio of 8:2 for BSCF and Co_3O_4 in the composite is the optimal composition. If the weight ratio between BSCF and Co_3O_4 is 9:1, then the cathode layer cannot adhere well to the electrolyte after firing, as shown in Fig. S7. This finding suggests that 10% Co_3O_4 is insufficient to bond BSCF to the electrolyte. When the weight ratio for Co_3O_4 increases to 30%, that is, the weight ratio between BSCF and Co_3O_4 is 7:3, the cathode layer can adhere to the electrolyte layer. However, the fuel cell performance is slightly lower than that of the cell using the BSCF + Co_3O_4 (8:2) cathode reported in the manuscript. Fig. S8 shows that the PPD of the cell using the BSCF + Co_3O_4 (7:3) cathode is 1250, 861, and 540 mW cm^{-2} at 700, 650, and 600°C, respectively. The PPD is lower than that of the cell using the aforementioned BSCF + Co_3O_4 (8:2) cathode.

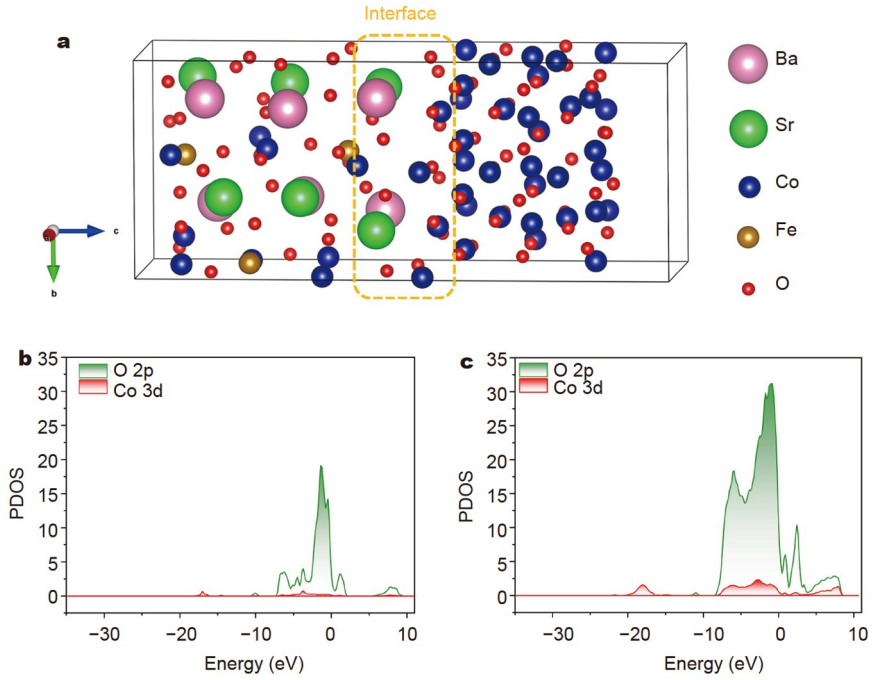

Figure 4 (a) Calculated configuration for BSCF-Co_3O_4 using first-principles; calculated partial DOS (PDOS) for Co 3d and O 2p orbitals for (b) BSCF and (c) BSCF + Co_3O_4.

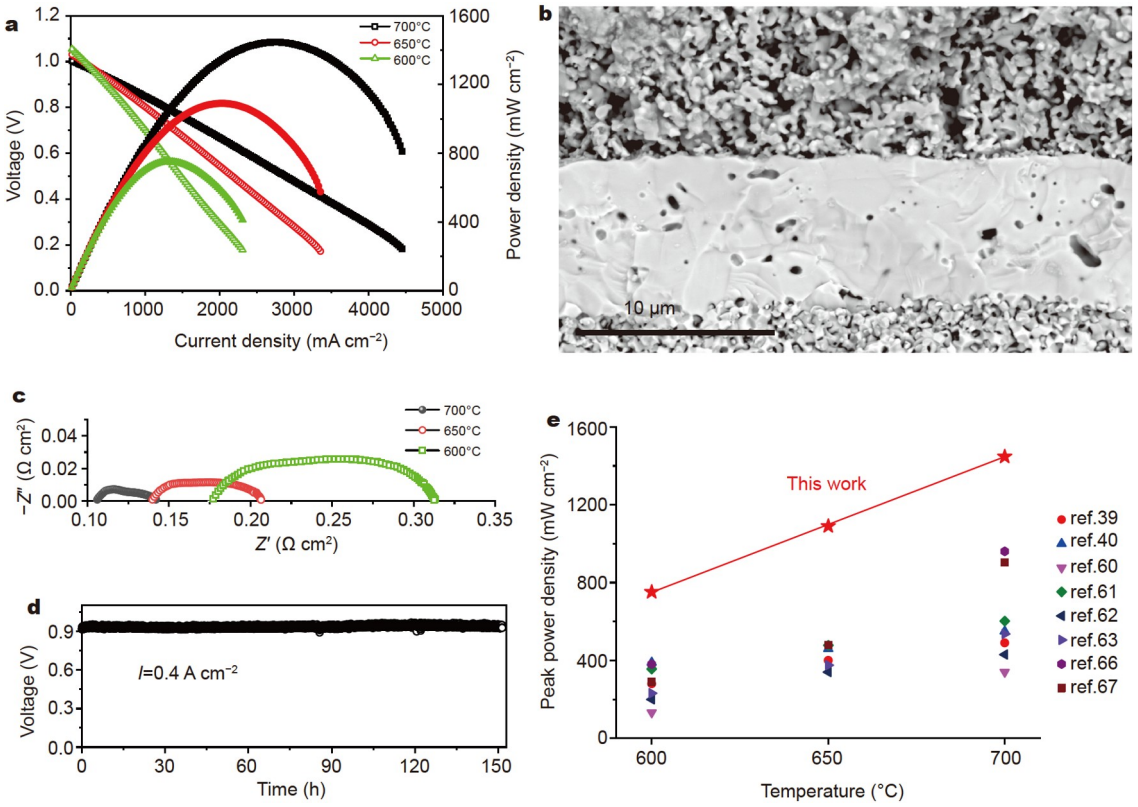

Figure 5 (a) *I-V* and power density curves for an H-SOFC using a BSCF + Co_3O_4 cathode; (b) cross-sectional view for the tested cell; (c) EIS plots for the cell tested at different temperatures; (d) electrochemical stability test for the cell operated at 600°C; (e) comparison of the performance of the current cell (NiO + BCZY/BCZY (14 μm)/BSCF + Co_3O_4) with H-SOFCs using BSCF cathodes reported in the literature: NiO + $BaCe_{0.8}Y_{0.2}O_3$/$BaCe_{0.8}Y_{0.2}O_3$ (30 μm)/BSCF [39]; NiO + $BaCe_{0.9}Y_{0.1}O_3$/$BaCe_{0.9}Y_{0.1}O_3$ (20 μm)/BSCF + $BaCe_{0.9}Y_{0.1}O_3$ [40]; NiO + $BaCe_{0.8}Sm_{0.2}O_3$/$BaCe_{0.8}Sm_{0.2}O_3$ (50 μm)/BSCF + $BaCe_{0.8}Sm_{0.2}O_3$ [60]; NiO + BCZY/BCZY (N/A)/BSCF [61]; NiO + $BaCe_{0.8}Sm_{0.2}F_{0.1}O_3$/$BaCe_{0.8}Sm_{0.2}F_{0.1}O_3$ (50 μm)/$Ba_{0.5}Sr_{0.5}Co_{0.8}Fe_{0.2}O_{2.9}F_{0.1}$ + $BaCe_{0.8}Sm_{0.2}F_{0.1}O_3$ [62]; NiO + BCZY/BCZY (N/A)/BSCF [63]; NiO + BCZY/BCZY (14 μm)/BSCF + BCZY [66]; NiO + BCZY/BCZY (10 μm)/BSCF + BCZY [67].

Fig. 5b shows the cross-sectional view of the cell after testing, indicating that the BSCF + Co_3O_4 cathode layer still adheres well to the electrolyte without detectable delamination. The above elemental analysis presented in Fig. 2b indicates that Co_3O_4 particles are dispersed at the entire cathode, extending the BSCF-Co_3O_4 interface and promoting the cathode reactions. The electrochemical impedance spectroscopy (EIS) plots shown in Fig. 5c indicate that the polarization resistance (R_p) of the cell is 0.036, 0.067, and 0.137 Ω cm^2 at 700, 650, and 600°C, respectively. These values are smaller than those of the BSCF-based cathodes for H-SOFCs, which are generally in the range of 0.1 to 0.4 Ω cm^2 at 700°C [39,40,60–63]. One factor for the substantially reduced R_p is the improved ORR activity of the BSCF + Co_3O_4 compared with the aforementioned BSCF. The other factor is the improved contact between the cathode and electrolyte layers, facilitating charge transfers and thus reducing R_p. No proton-conducting phase was added, but the BSCF + Co_3O_4 cathode still demonstrated good activity due to the following two reasons. First, the migrations of oxygen ions and protons are involved in the cathode reaction in the cathode for H-SOFCs [25]. Therefore, the cathode may show decent performance if the oxygen ion conduction is sufficiently high, and BSCF is a material containing the aforementioned characteristics. Second, recent reports [64,65] indicate that BSCF could show some proton conduction in the wet atmosphere and H_2O is produced at the cathode side for H-SOFCs that could trigger the proton conduction in BSCF. Therefore, the potential proton conduction in BSCF could further improve the cathode performance. In addition to the excellent fuel cell output and low R_p, the cell with the BSCF + Co_3O_4 cathode exhibits good long-term stability. Fig. 5d shows that the fuel cell works for approximately 150 h under the testing condition and no detectable degradation can be observed. Stability is one of the major concerns for BSCF. The stability of the BSCF phase in the BSCF + Co_3O_4 composite is partially improved with the protection of Co_3O_4. The chemical stability of BSCF and BSCF + Co_3O_4 was examined by treating the powders in a 20% CO_2-containing atmosphere at 600°C for 3 h, and the results are presented in Fig. S9. The figure reveals that extra peaks corresponding to $BaCO_3$ and $SrCO_3$ are formed for BSCF and BSCF + Co_3O_4 after the treatment. This phenomenon suggests the presence of a reaction between BSCF and CO_2, and this reaction is also observed for the BSCF phase in the BSCF + Co_3O_4 composite. However, the relative intensities of the $BaCO_3$ and $SrCO_3$ peaks for the single BSCF are higher than that for the BSCF + Co_3O_4 composite, suggesting that the reaction between BSCF and CO_2 in the BSCF + Co_3O_4 composite is less severe compared with that in the single-phase BSCF. This result also indicates that the Co_3O_4 particles partially protect the BSCF phase in the composite, making it less reactive compared with the single-phase BSCF. Notably, the performance of the current fuel cell is substantially higher than other H-SOFCs using BSCF-based cathodes reported in the literature, as shown in Fig. 5e. Notably, the traditional way of solving the thermal mismatch problem for BSCF is to couple it with proton-conducting oxides. The previous reports indicated that the performance is moderate [39,40,60–63,66,67], which is far inferior to the current study, despite the adherence of BSCF-based cathode to the electrolyte. Compared with BSCF-based cathodes modified with other doping strategies [67,68] or noble metals [69], the current BSCF + Co_3O_4 cathode shows superior performance. This result suggests that the utilization of Co_3O_4 not only overcomes the thermal mismatch for BSCF but also enhances the cathode and fuel cell performances, providing a new way to reuse BSCF for H-SOFCs.

CONCLUSIONS

BSCF is a classical cathode for intermediate-temperature SOFCs, but its high thermal expansion complicates the contact between the BSCF and electrolyte. Coupling BSCF with proton-conducting oxides can mitigate this problem, but the interdiffusion of elements and the moderate electrochemical performance contribute to the unsatisfactory performance of this strategy. An alternative strategy of using Co_3O_4 to glue BSCF to the electrolyte has been proposed in the current study. The low melting point of Co_3O_4 allows the formation of a melting phase during the co-firing procedure of cathodes, thus bonding BSCF to the proton-conducting electrolyte layer. Compared with the pure BSCF that completely peeled off from the electrolyte after co-firing, the BSCF + Co_3O_4 mixture firmly adheres to the electrolyte without any delamination. Elemental analysis suggests a good distribution of cobalt oxides in the entire cathode, including the cathode-electrolyte interface. Further experimental studies and first-principles calculations indicate that the addition of Co_3O_4 promotes the catalytic activity of the cathode, leading to a high fuel cell performance of H-SOFCs using the BSCF + Co_3O_4 cathode. This study not only provides a new cathode candidate for H-SOFCs but also offers an interesting strategy to solve the thermal mismatch problems for some high-performing cathodes with high thermal expansions.

Received 5 July 2022; accepted 30 August 2022; published online 28 November 2022

1 Zhou Y, Guan X, Zhou H, *et al.* Strongly correlated perovskite fuel cells. Nature, 2016, 534: 231–234
2 Boldrin P, Brandon NP. Progress and outlook for solid oxide fuel cells for transportation applications. Nat Catal, 2019, 2: 571–577
3 Shin JF, Xu W, Zanella M, *et al.* Self-assembled dynamic perovskite composite cathodes for intermediate temperature solid oxide fuel cells. Nat Energy, 2017, 2: 16214
4 Zhang Y, Knibbe R, Sunarso J, *et al.* Recent progress on advanced materials for solid-oxide fuel cells operating below 500°C. Adv Mater, 2017, 29: 1700132
5 Xi X, Fan Y, Zhang J, *et al. In situ* construction of hetero-structured perovskite composites with exsolved Fe and Cu metallic nanoparticles as efficient CO_2 reduction electrocatalysts for high performance solid oxide electrolysis cells. J Mater Chem A, 2022, 10: 2509–2518
6 Chen M, Xie X, Guo J, *et al.* Space charge layer effect at the platinum anode/$BaZr_{0.9}Y_{0.1}O_{3-\delta}$ electrolyte interface in proton ceramic fuel cells. J Mater Chem A, 2020, 8: 12566–12575
7 Zvonareva I, Fu XZ, Medvedev D, *et al.* Electrochemistry and energy conversion features of protonic ceramic cells with mixed ionic-electronic electrolytes. Energy Environ Sci, 2022, 15: 439–465
8 Gu H, Xu M, Song Y, *et al.* $SrCo_{0.8}Ti_{0.1}Ta_{0.1}O_{3-\delta}$ perovskite: A new highly active and durable cathode material for intermediate-temperature solid oxide fuel cells. Compos Part B-Eng, 2021, 213: 108726
9 Liu Z, Cheng D, Zhu Y, *et al.* Robust bifunctional phosphorus-doped perovskite oxygen electrode for reversible proton ceramic electrochemical cells. Chem Eng J, 2022, 450: 137787
10 Dai H, Kou H, Wang H, *et al.* Electrochemical performance of protonic ceramic fuel cells with stable $BaZrO_3$-based electrolyte: A mini-review. Electrochem Commun, 2018, 96: 11–15
11 Chen M, Chen D, Wang K, *et al.* Densification and electrical conducting behavior of $BaZr_{0.9}Y_{0.1}O_{3-\delta}$ proton conducting ceramics with NiO additive. J Alloys Compd, 2019, 781: 857–865
12 Medvedev DA, Lyagaeva JG, Gorbova EV, *et al.* Advanced materials for

SOFC application: Strategies for the development of highly conductive and stable solid oxide proton electrolytes. Prog Mater Sci, 2016, 75: 38–79
13 Duan C, Tong J, Shang M, *et al.* Readily processed protonic ceramic fuel cells with high performance at low temperatures. Science, 2015, 349: 1321–1326
14 Ding H, Wu W, Jiang C, *et al.* Self-sustainable protonic ceramic electrochemical cells using a triple conducting electrode for hydrogen and power production. Nat Commun, 2020, 11: 1907
15 Dai H, Yin Y, Li X, *et al.* A new Sc-doped $La_{0.5}Sr_{0.5}MnO_{3-\delta}$ cathode allows high performance for proton-conducting solid oxide fuel cells. Sustain Mater Technol, 2022, 32: e00409
16 Li P, Yang W, Tian C, *et al.* Electrochemical performance of $La_2NiO_{4+\delta}$-$Ce_{0.55}La_{0.45}O_{2-\delta}$ as a promising bifunctional oxygen electrode for reversible solid oxide cells. J Adv Ceram, 2021, 10: 328–337
17 Fu XZ, Luo JL, Sanger AR, *et al.* Y-doped $BaCeO_{3-\delta}$ nanopowders as proton-conducting electrolyte materials for ethane fuel cells to co-generate ethylene and electricity. J Power Sources, 2010, 195: 2659–2663
18 Han D, Uemura S, Hiraiwa C, *et al.* Detrimental effect of sintering additives on conducting ceramics: Yttrium-doped barium zirconate. ChemSusChem, 2018, 11: 4102–4113
19 Zhou C, Sunarso J, Song Y, *et al.* New reduced-temperature ceramic fuel cells with dual-ion conducting electrolyte and triple-conducting double perovskite cathode. J Mater Chem A, 2019, 7: 13265–13274
20 Wang Q, Hou J, Fan Y, *et al.* $Pr_2BaNiMnO_{7-\delta}$ double-layered Ruddlesden-Popper perovskite oxides as efficient cathode electrocatalysts for low temperature proton conducting solid oxide fuel cells. J Mater Chem A, 2020, 8: 7704–7712
21 Zhang L, Yin Y, Xu Y, *et al.* Tailoring $Sr_2Fe_{1.5}Mo_{0.5}O_{6-\delta}$ with Sc as a new single-phase cathode for proton-conducting solid oxide fuel cells. Sci China Mater, 2022, 65: 1485–1494
22 Wu S, Xu X, Li X, *et al.* High-performance proton-conducting solid oxide fuel cells using the first-generation Sr-doped $LaMnO_3$ cathode tailored with Zn ions. Sci China Mater, 2022, 65: 675–682
23 Song Y, Chen J, Yang M, *et al.* Realizing simultaneous detrimental reactions suppression and multiple benefits generation from nickel doping toward improved protonic ceramic fuel cell performance. Small, 2022, 18: 2200450
24 Song Y, Chen Y, Xu M, *et al.* A cobalt-free multi-phase nanocomposite as near-ideal cathode of intermediate-temperature solid oxide fuel cells developed by smart self-assembly. Adv Mater, 2020, 32: 1906979
25 Peng R, Wu T, Liu W, *et al.* Cathode processes and materials for solid oxide fuel cells with proton conductors as electrolytes. J Mater Chem, 2010, 20: 6218–6225
26 Xu X, Xu Y, Ma J, *et al.* Tailoring electronic structure of perovskite cathode for proton-conducting solid oxide fuel cells with high performance. J Power Sources, 2021, 489: 229486
27 Wang N, Hinokuma S, Ina T, *et al.* Mixed proton-electron-oxide ion triple conducting manganite as an efficient cobalt-free cathode for protonic ceramic fuel cells. J Mater Chem A, 2020, 8: 11043–11055
28 Tian H, Li W, Ma L, *et al.* Deconvolution of water-splitting on the triple-conducting Ruddlesden-Popper-phase anode for protonic ceramic electrolysis cells. ACS Appl Mater Interfaces, 2020, 12: 49574–49585
29 Zou D, Yi Y, Song Y, *et al.* The $BaCe_{0.16}Y_{0.04}Fe_{0.8}O_{3-\delta}$ nanocomposite: A new high-performance cobalt-free triple-conducting cathode for protonic ceramic fuel cells operating at reduced temperatures. J Mater Chem A, 2022, 10: 5381–5390
30 Yin Y, Dai H, Yu S, *et al.* Tailoring cobalt-free $La_{0.5}Sr_{0.5}FeO_{3-\delta}$ cathode with a nonmetal cation-doping strategy for high-performance proton-conducting solid oxide fuel cells. SusMat, 2022, 2: 607–616
31 Ren R, Wang Z, Meng X, *et al.* Tailoring the oxygen vacancy to achieve fast intrinsic proton transport in a perovskite cathode for protonic ceramic fuel cells. ACS Appl Energy Mater, 2020, 3: 4914–4922
32 Song Y, Chen Y, Wang W, *et al.* Self-assembled triple-conducting nanocomposite as a superior protonic ceramic fuel cell cathode. Joule, 2019, 3: 2842–2853
33 Tarutin AP, Lyagaeva JG, Medvedev DA, *et al.* Recent advances in layered $Ln_2NiO_{4+\delta}$ nickelates: Fundamentals and prospects of their applications in protonic ceramic fuel and electrolysis cells. J Mater Chem A, 2021, 9: 154–195
34 Tao Z, Xu X, Bi L. Density functional theory calculations for cathode materials of proton-conducting solid oxide fuel cells: A mini-review. Electrochem Commun, 2021, 129: 107072
35 Bu Y, Joo S, Zhang Y, *et al.* A highly efficient composite cathode for proton-conducting solid oxide fuel cells. J Power Sources, 2020, 451: 227812
36 Bae K, Jang DY, Choi HJ, *et al.* Demonstrating the potential of yttrium-doped barium zirconate electrolyte for high-performance fuel cells. Nat Commun, 2017, 8: 14553
37 Yin Y, Yu S, Dai H, *et al.* Triggering interfacial activity of the traditional $La_{0.5}Sr_{0.5}MnO_3$ cathode with Co-doping for proton-conducting solid oxide fuel cells. J Mater Chem A, 2022, 10: 1726–1734
38 Zhou W, Ran R, Shao Z. Progress in understanding and development of $Ba_{0.5}Sr_{0.5}Co_{0.8}Fe_{0.2}O_{3-\delta}$-based cathodes for intermediate-temperature solid-oxide fuel cells: A review. J Power Sources, 2009, 192: 231–246
39 Guo Y, Lin Y, Ran R, *et al.* Zirconium doping effect on the performance of proton-conducting $BaZr_yCe_{0.8-y}Y_{0.2}O_{3-\delta}$ ($0.0 \le y \le 0.8$) for fuel cell applications. J Power Sources, 2009, 193: 400–407
40 Lin Y, Ran R, Zheng Y, *et al.* Evaluation of $Ba_{0.5}Sr_{0.5}Co_{0.8}Fe_{0.2}O_{3-\delta}$ as a potential cathode for an anode-supported proton-conducting solid-oxide fuel cell. J Power Sources, 2008, 180: 15–22
41 Zhang Y, Chen B, Guan D, *et al.* Thermal-expansion offset for high-performance fuel cell cathodes. Nature, 2021, 591: 246–251
42 Han X, Cheng F, Chen C, *et al.* A Co_3O_4@MnO_2/Ni nanocomposite as a carbon- and binder-free cathode for rechargeable Li-O_2 batteries. Inorg Chem Front, 2016, 3: 866–871
43 Wang W, Wang Z, Hu Y, *et al.* A potential-driven switch of activity promotion mode for the oxygen evolution reaction at Co_3O_4/NiO_xH_y interface. eScience, 2022, 2: 438–444
44 Zhang H, Liu H, Cong Y, *et al.* Investigation of $Sm_{0.5}Sr_{0.5}CoO_{3-\delta}$/$Co_3O_4$ composite cathode for intermediate-temperature solid oxide fuel cells. J Power Sources, 2008, 185: 129–135
45 Bi L, Shafi SP, Da'as EH, *et al.* Tailoring the cathode-electrolyte interface with nanoparticles for boosting the solid oxide fuel cell performance of chemically stable proton-conducting electrolytes. Small, 2018, 14: 1801231
46 Kresse G, Furthmüller J. Efficient iterative schemes for *ab initio* total-energy calculations using a plane-wave basis set. Phys Rev B, 1996, 54: 11169–11186
47 Dan X, Wang C, Xu X, *et al.* Improving the sinterability of CeO_2 by using plane-selective nanocubes. J Eur Ceramic Soc, 2019, 39: 4429–4434
48 Xi X, Liu J, Fan Y, *et al.* Reducing d-p band coupling to enhance CO_2 electrocatalytic activity by Mg-doping in $Sr_2FeMoO_{6-\delta}$ double perovskite for high performance solid oxide electrolysis cells. Nano Energy, 2021, 82: 105707
49 Kilner JA, Burriel M. Materials for intermediate-temperature solid-oxide fuel cells. Annu Rev Mater Res, 2014, 44: 365–393
50 Broemme ADD. Correlation between thermal expansion and Seebeck coefficient in polycrystalline Co_3O_4. IEEE Trans Elect Insul, 1991, 26: 49–52
51 Zhang H, Yang W. Highly efficient electrocatalysts for oxygen reduction reaction. Chem Commun, 2007, 4215
52 Zhi M, Zhou G, Hong Z, *et al.* Single crystalline $La_{0.5}Sr_{0.5}MnO_3$ microcubes as cathode of solid oxidefuel cell. Energy Environ Sci, 2011, 4: 139–144
53 Xu Y, Xu X, Bi L. A high-entropy spinel ceramic oxide as the cathode for proton-conducting solid oxide fuel cells. J Adv Ceram, 2022, 11: 794–804
54 Zhou M, Liu J, Ye Y, *et al.* Enhancing the intrinsic activity and stability of perovskite cobaltite at elevated temperature through surface stress. Small, 2021, 17: 2104144
55 Ji Q, Bi L, Zhang J, *et al.* The role of oxygen vacancies of ABO_3 perovskite oxides in the oxygen reduction reaction. Energy Environ Sci, 2020, 13: 1408–1428
56 Xi X, Liu J, Luo W, *et al.* Unraveling the enhanced kinetics of

$Sr_2Fe_{1+x}Mo_{1-x}O_{6-\delta}$ electrocatalysts for high-performance solid oxide cells. Adv Energy Mater, 2021, 11: 2102845
57 Chen C, Wang XT, Zhong JH, *et al.* Epitaxially grown heterostructured $SrMn_3O_{6-x}$-$SrMnO_3$ with high-valence $Mn^{3+/4+}$ for improved oxygen reduction catalysis. Angew Chem Int Ed, 2021, 60: 22043–22050
58 Muñoz-García AB, Tuccillo M, Pavone M. Computational design of cobalt-free mixed proton-electron conductors for solid oxide electrochemical cells. J Mater Chem A, 2017, 5: 11825–11833
59 Hong WT, Stoerzinger KA, Lee YL, *et al.* Charge-transfer-energy-dependent oxygen evolution reaction mechanisms for perovskite oxides. Energy Environ Sci, 2017, 10: 2190–2200
60 Ranran P, Yan W, Lizhai Y, *et al.* Electrochemical properties of intermediate-temperature SOFCs based on proton conducting Sm-doped $BaCeO_3$ electrolyte thin film. Solid State Ion, 2006, 177: 389–393
61 Wan TT, Zhu AK, Li HB, *et al.* Performance variability of $Ba_{0.5}Sr_{0.5}Co_{0.8}Fe_{0.2}O_{3-\delta}$ cathode on proton-conducting electrolyte SOFCs with Ag and Au current collectors. Rare Met, 2018, 37: 633–641
62 Xie Y, Shi N, Huan D, *et al.* A stable and efficient cathode for fluorine-containing proton-conducting solid oxide fuel cells. ChemSusChem, 2018, 11: 3423–3430
63 Guan B, Lü Z, Wang G, *et al.* A performance study of solid oxide fuel cells with $BaZr_{0.1}Ce_{0.7}Y_{0.2}O_{3-\delta}$ electrolyte developed by spray-modified pressing method. Fuel Cells, 2012, 12: 141–145
64 Grimaud A, Mauvy F, Bassat JM, *et al.* Hydration properties and rate determining steps of the oxygen reduction reaction of perovskite-related oxides as H^+-SOFC cathodes. J Electrochem Soc, 2012, 159: B683–B694
65 Sun S, Cheng Z. Electrochemical behaviors for Ag, LSCF and BSCF as oxygen electrodes for proton conducting IT-SOFC. J Electrochem Soc, 2017, 164: F3104–F3113
66 Liu W, Kou H, Wang X, *et al.* Improving the performance of the $Ba_{0.5}Sr_{0.5}Co_{0.8}Fe_{0.2}O_{3-\delta}$ cathode for proton-conducting SOFCs by microwave sintering. Ceramics Int, 2019, 45: 20994–20998
67 Xu X, Wang H, Fronzi M, *et al.* Tailoring cations in a perovskite cathode for proton-conducting solid oxide fuel cells with high performance. J Mater Chem A, 2019, 7: 20624–20632
68 Li X, Liu Y, Liu W, *et al.* Mo-doping allows high performance for a perovskite cathode applied in proton-conducting solid oxide fuel cells. Sustain Energy Fuels, 2021, 5: 4261–4267
69 Lin Y, Ran R, Shao Z. Silver-modified $Ba_{0.5}Sr_{0.5}Co_{0.8}Fe_{0.2}O_{3-\delta}$ as cathodes for a proton conducting solid-oxide fuel cell. Int J Hydrogen Energy, 2010, 35: 8281–8288

Acknowledgements This work was supported by the National Natural Science Foundation of China (51972183), the Hundred Youth Talents Program of Hunan, and the Startup Funding for Talents at the University of South China.

Author contributions Bi L designed the study. Yang X and Yu S performed the experiments. Yin Y performed the DFT calculations and analyzed the data. Bi L wrote the manuscript with other co-authors, and all authors discussed the results and provided their approval for the final version.

Conflict of interest The authors declare that they have no conflict of interest.

Supplementary information Supporting data are available in the online version of the paper.

Xuan Yang is an undergraduate student in the group of Professor Lei Bi at the University of South China. Her research activities mainly focus on the synthesis and design of new cathode materials for H-SOFCs, revealing the relationship between the structures of materials and their electrochemical performance.

Yanru Yin is a staff researcher in the group of Professor Lei Bi at the University of South China. Her research interest is to tailor the structures and properties of proton-conducting oxides, aiming to understand the transportation mechanism of charge carriers in proton-conducting oxides and then boost the performance of H-SOFCs.

Lei Bi is a full professor at the University of South China and leads a research group working on H-SOFCs, using both the first-principles calculation method and experimental approaches. He has been working in the field of H-SOFCs for more than 15 years. His research interests cover the development and optimization of key materials for H-SOFCs and the new technologies for fuel cell fabrications.

通过Co_3O_4将$Ba_{0.5}Sr_{0.5}Co_{0.8}Fe_{0.2}O_{3-\delta}$进行粘合以作为质子导体固体氧化物燃料电池的阴极

杨璇[†], 尹燕儒[†], 于守富, 毕磊[*]

摘要 $Ba_{0.5}Sr_{0.5}Co_{0.8}Fe_{0.2}O_{3-\delta}$ (BSCF) + Co_3O_4复合材料作为质子导体固体氧化物燃料电池(H-SOFC)的阴极为在不影响阴极性能的前提下解决阴极与电解质之间热匹配的问题提供了一种新的策略. BSCF是中温氧离子导体SOFC中受到广泛认可的一种阴极材料, 但其在H-SOFC中的表现并不突出, 其中一个主要的原因是由于BSCF较高的热膨胀系数使其与电解质的接触不好. 在本研究中, 利用Co_3O_4熔点较低的特性将BSCF阴极粘结到电解质上, 以缓解BSCF与电解质之间接触不好的问题. 此外, 实验研究和第一性原理计算都证明了Co_3O_4的添加有效地增强了BSCF阴极的催化活性, 从而使该阴极展现出良好的电化学性能以及燃料电池输出性能.

